Periodic Emission from the Gamma-Ray Binary 1FGL J1018.6–5856

The Fermi LAT Collaboration

Science **335**, 189 (2012);
DOI: 10.1126/science.1213974

Science (print ISSN 0036-8075; online ISSN 1095-9203) is published weekly, except the last week in December, by the American Association for the Advancement of Science, 1200 New York Avenue NW, Washington, DC 20005.

27. Y. Qian, M. G. Flanner, L. R. Leung, W. Wang, *Atmos. Chem. Phys.* **11**, 1929 (2011).
28. M. Kopacz *et al.*, *Atmos. Chem. Phys.* **11**, 2837 (2011).
29. D. Shindell *et al.*, *J. Geophys. Res.* **115**, D19110 (2010).
30. G. A. Meehl, J. M. Arblaster, W. D. Collins, *J. Clim.* **21**, 2869 (2008).
31. C. Wang, D. Kim, A. M. L. Ekman, M. C. Barth, P. J. Rasch, *Geophys. Res. Lett.* **36**, L21704 (2009).
32. V. Ramanathan *et al.*, *Proc. Natl. Acad. Sci. U.S.A.* **102**, 5326 (2005).
33. V. Ramanathan, G. Carmichael, *Nat. Geosci.* **1**, 221 (2008).
34. C. D. Mathers, D. Loncar, *PLoS Med.* **3**, e442 (2006).
35. J. S. Fuglestvedt *et al.*, *Atmos. Environ.* **44**, 4648 (2010).
36. R. S. J. Tol, *Economics: The Open-Access, Open-Assessment E-Journal* **2**, 1 (2008).
37. International Energy Agency, "Building the Cost Curves for the Industrial Sources of Non-CO2 Greenhouse Gases" (IEA Greenhouse Gas R&D Programme Cheltenham, UK, 2003).
38. L. Höglund-Isaksson, W. Winiwarter, A. Tohka, "Potentials and costs for mitigation of non-CO2 greenhouse gases in the European Union until 2030—Methodology" (IIASA Report, Laxenburg, Austria, 2010).
39. M. Amann *et al.*, *Environ. Model. Softw.* **26**, 1489 (2011).
40. J. J. West, A. M. Fiore, *Environ. Sci. Technol.* **39**, 4685 (2005).
41. www.globalmethanefund.org; accessed 23 May 2011.
42. J. Hansen *et al.*, *Proc. Natl. Acad. Sci. U.S.A.* **103**, 14288 (2006).

Acknowledgments: Funding was provided by UNEP and the World Meteorological Organization (WMO), NASA's Applied Sciences and Atmospheric Chemistry Modeling and Analysis Programs, and the Clean Air Task Force to IIASA. We thank all the authors and reviewers who contributed to the UNEP/WMO Integrated Assessment of Black Carbon and Tropospheric Ozone.

Supporting Online Material

www.sciencemag.org/cgi/content/full/335/6065/183/DC1
Materials and Methods
Figs. S1 to S6
Tables S1 to S5
References

20 June 2011; accepted 28 November 2011
10.1126/science.1210026

Periodic Emission from the Gamma-Ray Binary 1FGL J1018.6–5856

The Fermi LAT Collaboration*

Gamma-ray binaries are stellar systems containing a neutron star or black hole, with gamma-ray emission produced by an interaction between the components. These systems are rare, even though binary evolution models predict dozens in our Galaxy. A search for gamma-ray binaries with the Fermi Large Area Telescope (LAT) shows that 1FGL J1018.6–5856 exhibits intensity and spectral modulation with a 16.6-day period. We identified a variable x-ray counterpart, which shows a sharp maximum coinciding with maximum gamma-ray emission, as well as an O6V((f)) star optical counterpart and a radio counterpart that is also apparently modulated on the orbital period. 1FGL J1018.6–5856 is thus a gamma-ray binary, and its detection suggests the presence of other fainter binaries in the Galaxy.

Two types of interacting binaries containing compact objects are expected to emit gamma rays (*1*): microquasars—accreting black holes or neutron stars with relativistic jets (*2*)—and rotation-powered pulsars interacting with the wind of a binary companion (*3*). Microquasars should typically be powerful x-ray sources when active, and hence such gamma ray–emitting systems may already be known x-ray binaries. Indeed, the bright x-ray source Cygnus X-3 is now known to be such a source (*4*, *5*). The existence of pulsars interacting with stellar companions of early spectral types is predicted as an initial stage in the formation of high-mass x-ray binaries (HMXBs) containing neutron stars (*6*). These interacting pulsars are predicted to be much weaker x-ray emitters and may not yet be known or classified x-ray sources. Gamma-ray binaries may thus not be as rare as they appear to be, and many systems may await detection.

A gamma-ray binary is expected to show orbitally modulated gamma-ray emission due to a combination of effects, including changes in viewing angle and, in eccentric orbits, the degree of the binary interaction, both of which depend on binary phase. Periodic gamma-ray modulation has indeed been seen in LS 5039 (period 3.9 days), LS I +61° 303 (26.5 days), and Cygnus X-3 (4.8 hours) (*4*, *7*, *8*), and gamma-ray emission is at least orbital phase–dependent for the PSR B1259–63 system (3.4 years) (*9*). However, the putative gamma-ray binary HESS J0632+057, for which a 321-day x-ray period is seen, has not yet been shown to exhibit periodic gamma-ray emission (*10*). PSR B1259–63 contains a pulsar, and LS 5039 and LS I +61° 303 are suspected, but not proved, to contain pulsars, whereas Cygnus X-3 is a black hole candidate. A search for periodic modulation of gamma-ray flux from LAT sources may thus lead to the detection of further gamma-ray binaries, potentially revealing the predicted HMXB precursor population. The first Fermi LAT (*11*) catalog of gamma-ray sources ("1FGL") contains 1451 sources (*12*), a large fraction of which do not have confirmed counterparts at other wavelengths and thus are potentially gamma-ray binaries.

To search for modulation, we used a weighted photon method to generate light curves for all 1FGL sources in the energy range 0.1 to 200 GeV (*13*). We then calculated power spectra for all sources. From an examination of these, in addition to modulation from the known binaries LS I +61° 303 and LS 5039, we noted the presence of a strong signal near a period of 16.6 days from 1FGL J1018.6–5856 (Fig. 1). 1FGL J1018.6–5856 has a cataloged 1- to 100-GeV flux of 2.9×10^{-8} photons cm^{-2} s^{-1}, making it one of the brighter LAT sources. The source's location at right ascension (R.A.) = 10^h 18.7^m, declination (decl.) = –58° 56.30′ (J2000; ±1.8′, 95% uncertainty) means that it lies close to the galactic plane (b = –1.7°), marking it as a good candidate for a binary system. 1FGL J1018.6–5856 has been noted to be positionally coincident with the supernova remnant G284.3–1.8 (*12*) and the TeV source HESS J1018–589 (*14*), although it has not been shown that these sources are actually related.

The modulation at a period of 16.6 days has a power more than 25 times the mean value of the power spectrum and has a false-alarm probability of 3×10^{-8}, taking into account the number of statistically independent frequency bins. From both the power spectrum itself (*15*) and from fitting the light curve, we derived a period of 16.58 ± 0.02 days. The folded light curve (Fig. 1) has a sharp peak together with additional broader modulation. We modeled this to determine the epoch of maximum flux T_{max} by fitting a function consisting of the sum of a sine wave and a Gaussian function, and obtained T_{max} = modified Julian date (MJD) 55403.3 ± 0.4.

The gamma-ray spectrum of 1FGL J1018.6–5856 shows substantial curvature through the LAT passband. To facilitate discussion of the lower-energy (<1 GeV) and higher-energy (>1 GeV) gamma rays, we adopted as our primary model a broken power law with photon indices $\Gamma_{0.1-1}$ and Γ_{1-10} for energies below and above 1 GeV, respectively. The best-fit values (*13*) are $\Gamma_{0.1-1} = 2.00 \pm 0.04_{stat} \pm 0.08_{syst}$ and $\Gamma_{1-10} = 3.09 \pm 0.06_{stat} \pm 0.12_{syst}$, along with an integral energy flux above 100 MeV of $(2.8 \pm 0.1_{stat} \pm 0.3_{syst}) \times 10^{-10}$ erg cm^{-2} s^{-1}. A power law with exponential cutoff (*7*, *8*), $dN/dE = N_0(E/\mathrm{GeV})^{-\Gamma} \exp(-E/E_c)$, gives an acceptable fit with $\Gamma = 1.9 \pm 0.1$ and $E_c = 2.5 \pm 0.3$ GeV (statistical errors only). Although this spectral shape is qualitatively similar to that of pulsars and of LS I +61° 303 and LS 5039, so far no detection of pulsed gamma-ray emission has been reported (*16*).

To investigate variability on the 16.6-day period, we folded the data into 10 uniform bins in orbital phase and then refit the broken power-law parameters within each phase bin. The resulting

*All authors with their affiliations appear at the end of this paper.

folded light curve (Fig. 2) indicates substantial variability in both the source brightness and spectral shape. In agreement with the detection of multiple harmonics of the orbital period in the power spectrum, there appear to be two primary features. For phases 0.2 to 0.6, the spectral curvature decreases and the peak of the spectral energy distribution lies below the LAT passband (indicated by $\Gamma_{0.1-1} > 2$). The onset of this soft spectrum is approximately coincident with a rise in x-ray emission and a peak in radio emission (see below). A weaker peak appears in the low-energy (< 1 GeV) γ-ray flux at phase 0.5 (Fig. 2). For the remaining phases, the LAT spectrum hardens with a comparatively sharp rise to, and fall from, a peak around 1 GeV ($\Gamma_{0.1-1} < 2$, $\Gamma_{1-10} > 2$). The variable spectral shape implies that only a modest fraction of the flux could represent steady magnetospheric emission from a pulsar.

We undertook observations of the location of 1FGL J1018.6–5856 covering the energy range 0.3 to 10 keV by means of the X-ray Telescope (XRT) onboard the Swift satellite. The first observation was obtained on 29 September 2009 with an exposure of 5 ks. A single source was detected in the XRT image (Fig. 3) within the LAT error circle. We then obtained additional observations from January to April 2011 to search for x-ray variability (*13*) and found large amplitude variability. Folded on the gamma-ray ephemeris (Fig. 4), there is a sharp peak in x-ray flux, coincident with the gamma-ray peak. However, in addition to this, a sine wave–like periodic modulation is also seen that peaks near phase 0.3 to 0.4.

Swift Ultraviolet/Optical Telescope (UVOT) (*17*) observations were obtained simultaneously with the x-ray observations. The x-ray source is positionally coincident with a bright source seen in the UVOT images (Fig. 3) (*13*), which in turn is coincident with a source in the U.S. Naval Observatory B1.0 catalog at (J2000.0) R.A. = $10^h\ 18^m\ 55^s.60 \pm 0.1''$, decl. = –58° 56′ 46.2″ ± 0.1″. Spectroscopic observations of the optical counterpart were performed using the South African Astronomical Observatory 1.9-m telescope and the 2.5-m telescope at the Las Campanas Observatory. Absorption lines due to H, He I, and He II identify it as an early-type star. We used a spectral atlas (*18*) to estimate the spectral type. He II λ4686 is present in absorption, which indicates a main-sequence star. The ratio of He II λ4541 to He I λ4471 implies an O6 spectral type. Weak emission is seen from N III but not He II, which indicates an ((f)) classification. We therefore estimate the spectral type as O6V((f)). This is very similar to the spectral type of LS 5039 (*19*). Interstellar absorption bands provide an estimate of the reddening, $E(B-V)$, defined as the relative absorption in the B and V optical bands; from the features at 4430 and 5780 Å, we derive $E(B-V) = 0.9$ and 1.6, respectively. Taking $V \sim 12.6$ from measurements with the All Sky Automated Survey (ASAS) (*20*), we derive a distance, d, to 1FGL J1018.6–5856 from Earth of 5 ± 2 kpc, allowing for uncertainties in the reddening and spectral classification.

Radio observations of the 1FGL J1018.6–5856 region were obtained with the Australia Telescope Compact Array (ATCA) at frequencies of 5.5 and 9 GHz. A faint radio source at R.A. = $10^h\ 18^m\ 55^s.580$, decl. = –58° 56′ 45.5″ (±0.1″ and 0.3″, respectively) is coincident with the stellar position. The radio source was clearly seen to be variable (Fig. 4). Unlike the gamma-ray and x-ray modulation, there is no obvious brightening in the radio at phase zero. Instead, it appears that the radio may be following the smoother sine wave–like component of the x-ray modulation.

1FGL J1018.6–5856 shares many properties with LS 5039. They are both fairly steady gamma-ray sources on long time scales, their periodic modulations have not shown large changes, and their optical counterparts are of a very similar spectral type. The x-ray light curve of LS 5039 appears to be highly repeatable (*21*, *22*), and the x-ray light curve of 1FGL J1018.6–5856 also shows repeatable behavior with a flux increase around phase 0 repeated over four orbital periods. The lack of variability in UV/optical brightness is also reminiscent of LS 5039 (*23*, *24*). This suggests that there is little ellipsoidal modulation of the primary star and hence that it substantially underfills its Roche lobe. On the other hand, the relative phasing of the gamma-ray spectral modulation and flux modulation differ from those of LS 5039 where the spectrum is softest when the flux is highest (*8*). Also, for LS 5039 the phases of maximum x-ray and gamma-ray do not coincide (*8*, *22*). The brightest peak in the folded gamma-ray light curve of 1FGL J1018.6–5856 at phase 0 is associated with the hardest gamma-ray spectrum and is coincident with x-ray flaring and minimum radio emission. Finally, 1FGL J1018.6–5856 has a much longer orbital period.

The gamma-ray modulation observed in 1FGL J1018.6–5856 could be due to anisotropic inverse Compton (IC) scattering between stellar photons and high-energy electrons that varies with orbital phase, as proposed for LS 5039 and LS I +61° 303 (*7*, *8*). However, the modulation amplitude is considerably lower in 1FGL J1018.6–5856 [$(f_{max} - f_{min})/(f_{max} + f_{min}) \approx 25\%$] relative to that of LS 5039 (≈ 60%). Modulation amplitude should increase with eccentricity and is highest for systems viewed edge-on (*25*); however, in the case of LS I +61° 303, the modulation fraction has been observed to undergo large changes (*26*). If the IC scattering interpretation is correct, then this implies that 1FGL J1018.6–5856 has both low inclination and low eccentricity. For comparison, the eccentricity of LS 5039 has been reported to be in the range of 0.3 to 0.5 (*19*, *27*, *28*). Although a low inclination angle implies that it would be difficult to measure the radial velocity of the companion from optical studies, the small Doppler shifts predicted would facilitate a pulsation search at GeV energies.

The gamma-ray spectral variability of 1FGL J1018.6–5856 over the orbit is also reminiscent of

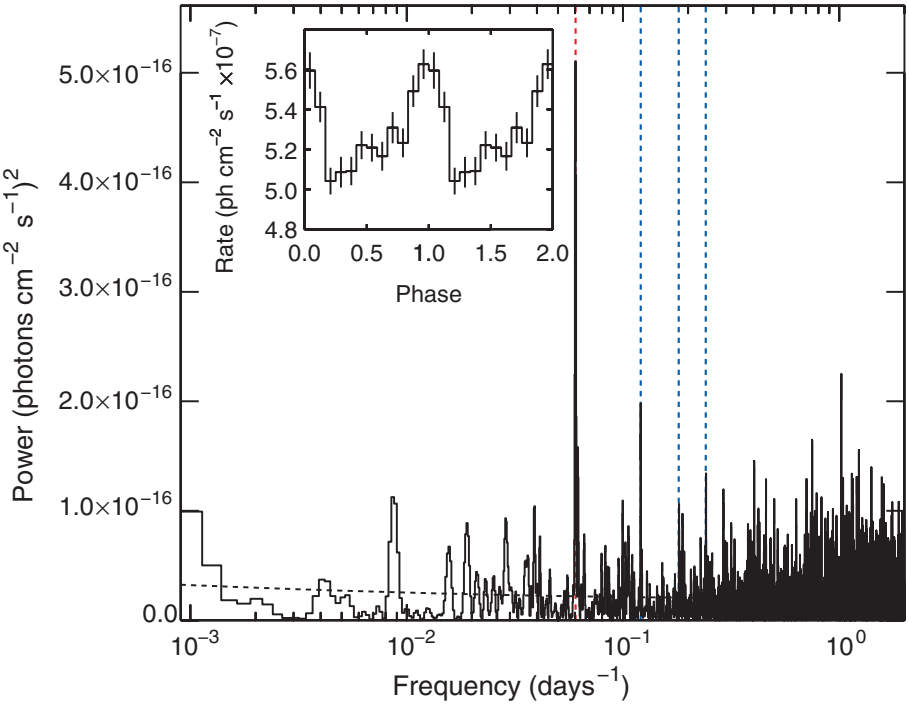

Fig. 1. Power spectrum of the LAT weighted photon light curve ($E > 100$ MeV) of 1FGL J1018.6–5856. The power spectrum is oversampled by a factor of 4 relative to its nominal resolution. The red dashed line indicates the 16.6-day period; the blue dashed lines are the second, third, and fourth harmonics of this. The dashed black line is a fit to the continuum power. The inset shows the weighted photon light curve folded on the 16.6-day period.

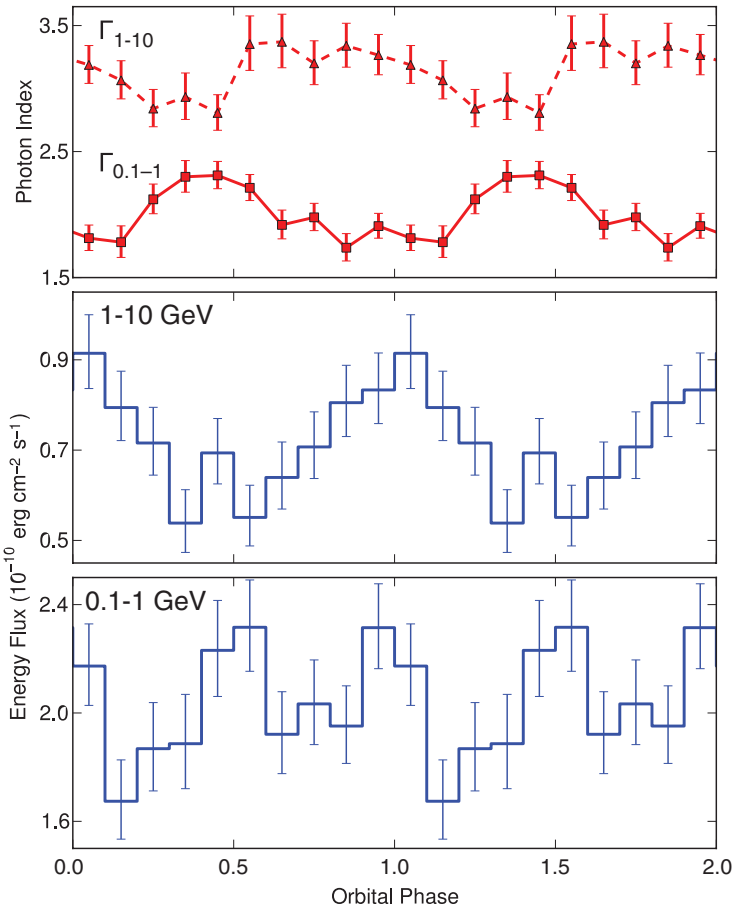

Fig. 2. The orbital modulation of the flux and spectral indices of 1FGL J1018.6–5856 in the 0.1 to 10 GeV band as measured with the Fermi LAT. $\Gamma_{0.1\text{–}1}$ and $\Gamma_{1\text{–}10}$ are photon spectral indices for energies below and above 1 GeV, respectively, using a broken power-law model.

LS 5039 but is unlike the behavior of LS I +61° 303. If the high-energy electron distribution remains constant along the orbit, spectral changes due to the anisotropic IC cross section are expected only if the inclination is substantial. In this case, harder spectra are expected to occur when the stellar photons are forward-scattered by the electrons (i.e., at inferior conjunction), which is also typically when the scattering rate is at its orbital minimum. However, for 1FGL J1018.6–5856 the hardness ratio and flux are correlated, unlike for LS 5039 (*8*). If periastron passage coincides with inferior conjunction, then a high photon density might compensate for the unfavorable interaction angle, but this requires fine-tuning of the orbital parameters. The spectral variability is more likely to reflect intrinsic variations—for instance, in the cooling of emitting particles. Moreover, both PSR B1259–63 and LS I +61° 303 (*7*, *9*) show that a simple model may not be correct. The phasing of gamma-ray maximum at GeV energies is not consistent with IC scattering on stellar photons, as it is delayed in both PSR B1259–63 and LS I +61° 303, implying that other mechanisms may be at work. For example, there could be other seed photon sources, Doppler boosting, or other radiative mechanisms at work.

The gamma-ray energy flux of 1FGL J1018.6–5856 implies a luminosity of $\sim 8 \times 10^{35}$ $(d/5\ \mathrm{kpc})^2$ ergs s^{-1} ($E > 100$ MeV), whereas the implied x-ray luminosity is highly variable with fluxes up to $\sim 10^{34}$ $(d/5\ \mathrm{kpc})^2$ ergs s^{-1}. For comparison, the gamma-ray luminosity of LS 5039 is $\sim 2 \times 10^{35}$ $(d/2.5\ \mathrm{kpc})^2$ ergs s^{-1} (*26*). This is somewhat surprising; relative to LS 5039, the orbital period of 1FGL J1018.6–5856 (longer by a factor of 4)

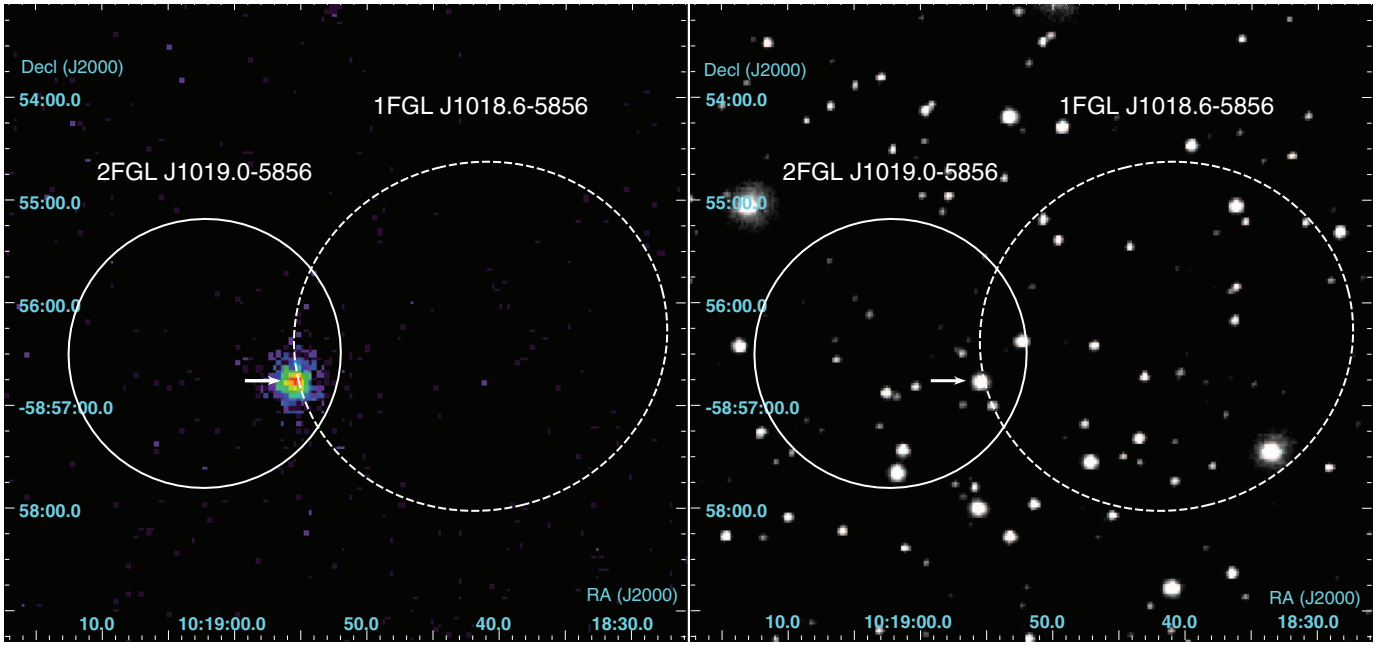

Fig. 3. Swift XRT x-ray (left) and UVOT-W1 (right) images of the region around 1FGL J1018.6–5856. The x-ray–optical counterpart is marked by an arrow near the center of both images. The LAT 95% confidence ellipses from the 1FGL (*12*) and 2FGL (*29*) catalogs are marked.

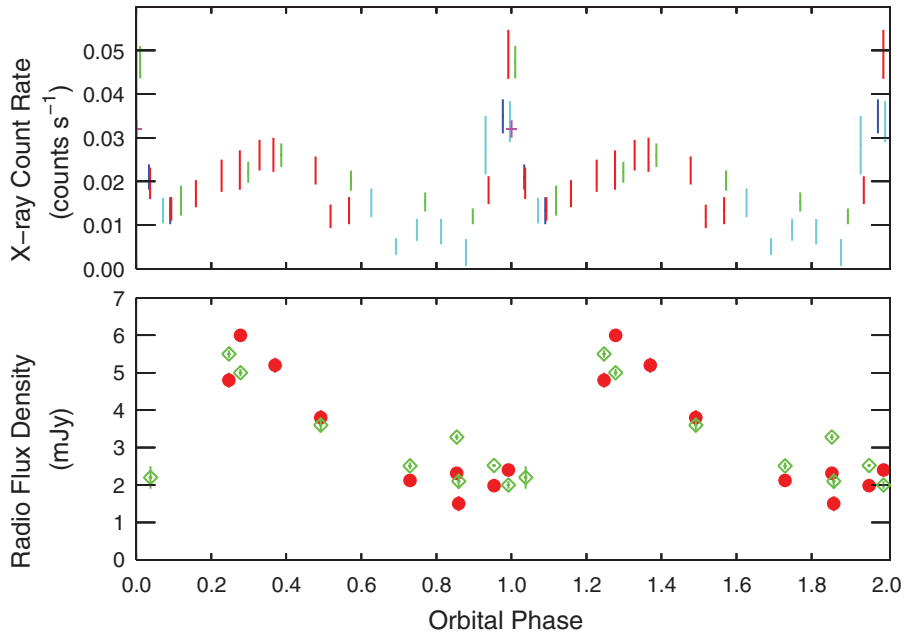

Fig. 4. X-ray (upper panel) and radio (lower panel) observations of 1FGL J1018.6–5856 folded on the orbital period. The x-ray data are from the Swift XRT and cover the energy range 0.3 to 10 keV. For the x-ray observations, the different colors indicate data taken from different 16.58-day orbital cycles. For the radio data, green diamonds indicate 9-GHz data and red circles 5.5-GHz data. The radio data are from the ATCA.

implies a major axis that is larger by a factor of 2.5, so that the mean stellar radiation density seen by the compact object is smaller by a factor of 6. The higher gamma-ray luminosity of 1FGL J1018.6–5856 indicates that the power injected in nonthermal particles must therefore be substantially higher in 1FGL J1018.6–5856 than in LS 5039. The similarity to LS 5039 suggests that we may be observing a rapidly rotating neutron star interacting with its companion. This raises the possibility that the neutron star rotation period might be detectable, as is the case with PSR B1259–63. However, our observations cannot definitely exclude an accreting neutron star or black hole.

References and Notes

1. I. F. Mirabel, *Science* **312**, 1759 (2006).
2. J. M. Paredes, J. Martí, M. Ribó, M. Massi, *Science* **288**, 2340 (2000).
3. G. Dubus, *Astron. Astrophys.* **456**, 801 (2006).
4. A. A. Abdo *et al.*; Fermi LAT Collaboration, *Science* **326**, 1512 (2009).
5. M. Tavani *et al.*, *Nature* **462**, 620 (2009).
6. E. J. A. Meurs, E. P. J. van den Heuvel, *Astron. Astrophys.* **226**, 88 (1989).
7. A. A. Abdo *et al.*, *Astrophys. J.* **701**, L123 (2009).
8. A. A. Abdo *et al.*, *Astrophys. J.* **706**, L56 (2009).
9. A. A. Abdo *et al.*, *Astrophys. J.* **736**, L11 (2011).
10. S. D. Bongiorno *et al.*, *Astrophys. J.* **737**, L11 (2011).
11. W. B. Atwood *et al.*, *Astrophys. J.* **697**, 1071 (2009).
12. A. A. Abdo *et al.*, *Astrophys. J. Suppl. Ser.* **188**, 405 (2010).
13. See supporting material on *Science* Online.
14. E. de Ona Wilhelmi *et al.*, paper presented at the 38th COSPAR Scientific Assembly, 23 July 2010, Bremen, Germany (paper E19-0082-10, poster Thu-286).
15. J. H. Horne, S. L. Baliunas, *Astrophys. J.* **302**, 757 (1986).
16. P. M. Saz Parkinson *et al.*, *Astrophys. J.* **725**, 571 (2010).
17. P. W. A. Roming *et al.*, *Space Sci. Rev.* **120**, 95 (2005).
18. N. R. Walborn, E. L. Fitzpatrick, *Publ. Astron. Soc. Pac.* **102**, 379 (1990).
19. M. V. McSwain *et al.*, *Astrophys. J.* **600**, 927 (2004).
20. G. Pojmański, *Acta Astronomica* **52**, 397 (2002).
21. T. Kishishita, T. Tanaka, Y. Uchiyama, T. Takahashi, *Astrophys. J.* **697**, L1 (2009).
22. T. Takahashi *et al.*, *Astrophys. J.* **697**, 592 (2009).
23. J. S. Clark *et al.*, *Astron. Astrophys.* **376**, 476 (2001).
24. J. Martí, P. Luque-Escamilla, J. L. Garrido, J. M. Paredes, R. Zamanov, *Astron. Astrophys.* **418**, 271 (2004).
25. G. Dubus, B. Cerutti, G. Henri, *Astron. Astrophys.* **477**, 691 (2008).
26. D. Hadasch, http://arxiv.org/abs/1111.0350 (2011).
27. J. Casares *et al.*, *Mon. Not. R. Astron. Soc.* **364**, 899 (2005).
28. G. E. Sarty *et al.*, *Mon. Not. R. Astron. Soc.* **411**, 1293 (2011).
29. The Fermi-LAT Collaboration, http://arxiv.org/abs/1108.1435 (2011).

Acknowledgments: The Fermi LAT Collaboration acknowledges support from a number of agencies and institutes for both development and the operation of the LAT as well as scientific data analysis. These include NASA and the U.S. Department of Energy (United States); CEA/Irfu and IN2P3/CNRS (France); ASI and INFN (Italy); MEXT, KEK, and JAXA (Japan); and the K. A. Wallenberg Foundation, the Swedish Research Council, and the National Space Board (Sweden). Additional support from INAF in Italy and CNES in France for science analysis during the operations phase is also gratefully acknowledged. Fermi LAT data are available from the Fermi Science Support Center (http://fermi.gsfc.nasa.gov/ssc). This work made use of data supplied by the UK Swift Science Data Centre at the University of Leicester. G.D. was supported by European Community contract ERC-StG-200911.

The Fermi LAT Collaboration

M. Ackermann,[1] M. Ajello,[1] J. Ballet,[2] G. Barbiellini,[3,4] D. Bastieri,[5,6] A. Belfiore,[7,8,9] R. Bellazzini,[10] B. Berenji,[1] R. D. Blandford,[1] E. D. Bloom,[1] E. Bonamente,[11,12] A. W. Borgland,[1] J. Bregeon,[10] M. Brigida,[13,14] P. Bruel,[15] R. Buehler,[1] S. Buson,[5,6] G. A. Caliandro,[16] R. A. Cameron,[1] P. A. Caraveo,[9] E. Cavazzuti,[17] C. Cecchi,[11,12] Ö. Çelik,[18,19,20] E. Charles,[1] S. Chaty,[2] A. Chekhtman,[21]† C. C. Cheung,[22]†‡ J. Chiang,[1] S. Ciprini,[12,23] R. Claus,[1] J. Cohen-Tanugi,[24] S. Corbel,[2,25] R. H. D. Corbet,[18,20]‡ S. Cutini,[17] A. de Luca,[26] P. R. den Hartog,[1] F. de Palma,[13,14] C. D. Dermer,[27] S. W. Digel,[1] E. do Couto e Silva,[1] D. Donato,[19,28] P. S. Drell,[1] A. Drlica-Wagner,[1] R. Dubois,[1] G. Dubus,[29] C. Favuzzi,[13,14] S. J. Fegan,[15] E. C. Ferrara,[18] W. B. Focke,[1] P. Fortin,[15] Y. Fukazawa,[30] S. Funk,[1] P. Fusco,[13,14] F. Gargano,[14] D. Gasparrini,[17] N. Gehrels,[18] S. Germani,[11,12] N. Giglietto,[13,14] F. Giordano,[13,14] M. Giroletti,[31] T. Glanzman,[1] G. Godfrey,[1] I. A. Grenier,[2] J. E. Grove,[27] S. Guiriec,[32] D. Hadasch,[16] Y. Hanabata,[30] A. K. Harding,[18] M. Hayashida,[1,33] E. Hays,[18] A. B. Hill,[34] R. E. Hughes,[35] G. Jóhannesson,[36] A. S. Johnson,[1] T. J. Johnson,[22]† T. Kamae,[1] H. Katagiri,[37] J. Kataoka,[38] M. Kerr,[1]‡§ J. Knödlseder,[39,40] M. Kuss,[10] J. Lande,[1] F. Longo,[3,4] F. Loparco,[13,14] M. N. Lovellette,[27] P. Lubrano,[11,12] M. N. Mazziotta,[14] J. E. McEnery,[18,28] P. F. Michelson,[1] W. Mitthumsiri,[1] T. Mizuno,[30] C. Monte,[13,14] M. E. Monzani,[1] A. Morselli,[41] I. V. Moskalenko,[1] S. Murgia,[1] T. Nakamori,[38] M. Naumann-Godo,[2] J. P. Norris,[42] E. Nuss,[24] M. Ohno,[43] T. Ohsugi,[44] A. Okumura,[1,43] N. Omodei,[1] E. Orlando,[1,45] M. Ozaki,[43] D. Paneque,[1,46] D. Parent,[47]† M. Pesce-Rollins,[10] M. Pierbattista,[2] F. Piron,[24] G. Pivato,[6] T. A. Porter,[1] S. Rainò,[13,14] R. Rando,[5,6] M. Razzano,[7,10] A. Reimer,[1,48] O. Reimer,[1,48] S. Ritz,[7] R. W. Romani,[1] M. Roth,[49] P. M. Saz Parkinson,[7] C. Sgrò,[10] E. J. Siskind,[50] G. Spandre,[10] P. Spinelli,[13,14] D. J. Suson,[51] H. Takahashi,[44] T. Tanaka,[1] J. G. Thayer,[1] J. B. Thayer,[1] D. J. Thompson,[18] L. Tibaldo,[5,6] M. Tinivella,[10] D. F. Torres,[16,52] G. Tosti,[11,12] E. Troja,[18]|| Y. Uchiyama,[1] T. L. Usher,[1] J. Vandenbroucke,[1] G. Vianello,[1,53] V. Vitale,[42,54] A. P. Waite,[1] B. L. Winer,[35] K. S. Wood,[27] M. Wood,[1] Z. Yang,[55,56] S. Zimmer,[55,56] M. J. Coe,[34] F. Di Mille,[57] P. G. Edwards,[58] M. D. Filipović,[59] J. L. Payne,[59] J. Stevens,[60] M. A. P. Torres[61]

[1]W. W. Hansen Experimental Physics Laboratory, Kavli Institute for Particle Astrophysics and Cosmology, Department of Physics and SLAC National Accelerator Laboratory, Stanford University, Stanford, CA 94305, USA. [2]Laboratoire AIM, CEA-IRFU/CNRS/Université Paris Diderot, Service d'Astrophysique, CEA Saclay, 91191 Gif-sur-Yvette, France. [3]Istituto Nazionale di Fisica Nucleare, Sezione di Trieste, I-34127 Trieste, Italy. [4]Dipartimento di Fisica, Università di Trieste, I-34127 Trieste, Italy. [5]Istituto Nazionale di Fisica Nucleare, Sezione di Padova, I-35131 Padova, Italy. [6]Dipartimento di Fisica "G. Galilei," Università di Padova, I-35131 Padova, Italy. [7]Santa Cruz Institute for Particle Physics, Department of Physics and Department of Astronomy and Astrophysics, University of California, Santa Cruz, CA 95064, USA. [8]Università degli Studi di Pavia, 27100 Pavia, Italy. [9]INAF–Istituto di Astrofisica Spaziale e Fisica Cosmica, I-20133 Milano, Italy. [10]Istituto Nazionale di Fisica Nucleare, Sezione di Pisa, I-56127 Pisa, Italy. [11]Istituto Nazionale di Fisica Nucleare, Sezione di Perugia, I-06123 Perugia, Italy. [12]Dipartimento di Fisica, Università degli Studi di Perugia, I-06123 Perugia, Italy. [13]Dipartimento di Fisica "M. Merlin" dell'Università e del Politecnico di Bari, I-70126 Bari, Italy. [14]Istituto Nazionale di Fisica Nucleare, Sezione di Bari, 70126 Bari, Italy. [15]Laboratoire Leprince-Ringuet, École Polytechnique, CNRS/IN2P3, Palaiseau, France. [16]Institut de Ciències de l'Espai (IEEE-CSIC), Campus UAB, 08193 Barcelona, Spain. [17]Agenzia Spaziale Italiana (ASI) Science Data Center, I-00044 Frascati (Roma), Italy. [18]NASA Goddard Space Flight Center, Greenbelt, MD 20771, USA. [19]Center for Research and Exploration in Space Science and Technology and NASA Goddard Space Flight Center, Greenbelt, MD 20771, USA. [20]Center for Space Sciences and Technology, University of Maryland Baltimore County, Baltimore, MD 21250, USA. [21]Artep Inc., 2922 Excelsior Springs Court, Ellicott City, MD 21042, USA. [22]National Research Council Research Associate, National Academy of Sciences, Washington, DC 20001, USA. [23]ASI Science Data Center, I-00044 Frascati (Roma), Italy. [24]Laboratoire Univers et Particules de Montpellier, Université Montpellier 2, CNRS/IN2P3, Montpellier, France. [25]Institut Universitaire de France, 75005 Paris, France. [26]Istituto Universitario di Studi Superiori, I-27100 Pavia, Italy. [27]Space Science Division, Naval Research Laboratory, Washington, DC 20375, USA. [28]Department of Physics and Department of Astronomy, University of Maryland, College Park, MD 20742, USA. [29]Institut de Planétologie et d'Astrophysique de Grenoble, Université Joseph Fourier-Grenoble 1/CNRS-INSU, UMR 5274, Grenoble F-38041, France. [30]Department of Physical Sciences, Hiroshima University, Higashi-Hiroshima, Hiroshima 739-8526, Japan. [31]INAF Istituto di Radioastronomia, 40129 Bologna, Italy. [32]Center for Space Plasma and Aeronomic Research, University of Alabama, Huntsville, AL 35899, USA. [33]Department of Astronomy, Graduate School of Science, Kyoto University,

Sakyo-ku, Kyoto 606-8502, Japan. [34]School of Physics and Astronomy, University of Southampton, Highfield, Southampton SO17 1BJ, UK. [35]Department of Physics, Center for Cosmology and Astro-Particle Physics, Ohio State University, Columbus, OH 43210, USA. [36]Science Institute, University of Iceland, IS-107 Reykjavik, Iceland. [37]College of Science, Ibaraki University, 2-1-1, Bunkyo, Mito 310-8512, Japan. [38]Research Institute for Science and Engineering, Waseda University, 3-4-1, Okubo, Shinjuku, Tokyo 169-8555, Japan. [39]CNRS, IRAP, F-31028 Toulouse Cedex 4, France. [40]GAHEC, Université de Toulouse, UPS-OMP, IRAP, Toulouse, France. [41]Istituto Nazionale di Fisica Nucleare, Sezione di Roma "Tor Vergata," I-00133 Roma, Italy. [42]Department of Physics, Boise State University, Boise, ID 83725, USA. [43]Institute of Space and Astronautical Science, JAXA, 3-1-1 Yoshinodai, Chuo-ku, Sagamihara, Kanagawa 252-5210, Japan. [44]Hiroshima Astrophysical Science Center, Hiroshima University, Higashi-Hiroshima, Hiroshima 739-8526, Japan. [45]Max-Planck-Institut für extraterrestrische Physik, 85748 Garching, Germany. [46]Max-Planck-Institut für Physik, D-80805 München, Germany. [47]Center for Earth Observing and Space Research, College of Science, George Mason University, Fairfax, VA 22030. [48]Institut für Astro- und Teilchenphysik and Institut für Theoretische Physik, Leopold-Franzens-Universität Innsbruck, A-6020 Innsbruck, Austria. [49]Department of Physics, University of Washington, Seattle, WA 98195, USA. [50]NYCB Real-Time Computing Inc., Lattingtown, NY 11560, USA. [51]Department of Chemistry and Physics, Purdue University Calumet, Hammond, IN 46323, USA. [52]Institució Catalana de Recerca i Estudis Avançats (ICREA), Barcelona, Spain. [53]Consorzio Interuniversitario per la Fisica Spaziale (CIFS), I-10133 Torino, Italy. [54]Dipartimento di Fisica, Università di Roma "Tor Vergata," I-00133 Roma, Italy. [55]Department of Physics, Stockholm University, AlbaNova, SE-106 91 Stockholm, Sweden. [56]Oskar Klein Centre for Cosmoparticle Physics, AlbaNova, SE-106 91 Stockholm, Sweden. [57]Australian Astronomical Observatory–Las Campanas Observatory, Colina, El Pino Casilla 601, La Serena, Chile. [58]Australia Telescope National Facility, CSIRO Astronomy and Space Science, Narrabri, NSW 2390, Australia. [59]University of Western Sydney, Locked Bag 1797, Penrith, NSW 2751, Australia. [60]CSIRO Astronomy and Space Science, Epping, NSW 1710, Australia. [61]Harvard-Smithsonian Center for Astrophysics, Cambridge, MA 02138, USA.

†Resident at Naval Research Laboratory, Washington, DC 20375, USA.
‡To whom correspondence should be addressed. E-mail: robin.corbet@nasa.gov (R.H.D.C.); kerrm@stanford.edu (M.K.); teddy.cheung.ctr@nrl.navy.mil (C.C.C.)
§Einstein Fellow.
‖NASA Postdoctoral Program Fellow.

Supporting Online Material
www.sciencemag.org/cgi/content/full/335/6065/189/DC1
Materials and Methods
Figs. S1 to S4
References (*30*–*46*)

14 September 2011; accepted 16 November 2011
10.1126/science.1213974

Universal Signatures of Fractionalized Quantum Critical Points

Sergei V. Isakov,[1] Roger G. Melko,[2] Matthew B. Hastings[3,4]*

Ground states of certain materials can support exotic excitations with a charge equal to a fraction of the fundamental electron charge. The condensation of these fractionalized particles has been predicted to drive unusual quantum phase transitions. Through numerical and theoretical analysis of a physical model of interacting lattice bosons, we establish the existence of such an exotic critical point, called XY*. We measure a highly nonclassical critical exponent $\eta = 1.493$ and construct a universal scaling function of winding number distributions that directly demonstrates the distinct topological sectors of an emergent Z_2 gauge field. The universal quantities used to establish this exotic transition can be used to detect other fractionalized quantum critical points in future model and material systems.

It is noteworthy that, in this age of high-energy accelerator experiments, certain types of fundamental quantum particles can only be studied in tabletop condensed-matter physics experiments. Consider, for example, the electron, carrying fundamental charge e. Unlike the proton, whose charge originates from quarks with fractional charge, no energy is sufficiently high to break up the charge of an electron. However, as demonstrated by the measurement of fractional Hall conductance, if one places an electron in certain clean two-dimensional (2D) materials in a strong magnetic field, its charge can break into fractions—$e/3$, $e/5$, and so on (*1*)—with each fractional charge arising from a quasiparticle emerging as an excitation of the ground state.

Such quasiparticles share all the important characteristics of real particles. In deconfined phases of matter with a gap to excitations, the quasiparticles can be separated a large distance from each other, making them well-defined localized objects with a sharp energy-momentum dispersion relation. For more than a decade, condensed-matter physicists have searched for fractionalized particles in systems other than Hall effect materials. Theoretical predictions have identified a class of low-temperature paramagnets, the quantum spin liquids, as holding particular promise for supporting them (*2*–*4*). However, experimental searches for these fractional charges and their parent spin-liquid vacuum remain unconvincing. This is partly a result of the difficulty in constructing measurements that are able to identify their experimental signatures in the variety of materials—ranging from fabricated solid-state devices to organic magnets—thought to harbor spin-liquid states (*5*). An interesting recent experimental candidate is a set of materials that may display fractional particles with a gapless Fermi surface (*6*–*11*), where interaction between quasiparticles makes it problematic to even define a fractionalized excitation (*12*). In bosonic systems, such interacting gapless fractional quasiparticles have been proposed to mediate quantum critical points that exist in certain order-to-order transitions (*13*). For these Landau-violating critical points (which rely on long-wavelength fluctuations of fractional particles), signatures of the fractionalization are manifest in universal quantities, such as critical exponents, instead of specific material-dependent quantities.

A major goal of the theoretical community has been to demonstrate the existence of these "deconfined" quantum critical points in realistic microscopic models, with the use of large-scale numerical simulation (*14*). In this work, we used quantum Monte Carlo (QMC) to study deconfined quantum criticality in the context of an order-to-disorder transition between a superfluid and a gapped spin-liquid state, in a physical model of lattice bosons. The model we examine is a variant of the Bose-Hubbard Hamiltonian, introduced in (*15*), which is a simple model of hard-core bosons hopping (with strength t) on a 2D kagome lattice with an energetic constraint (V) favoring three bosons per hexagonal lattice plaquette: $H = -t\sum_{\langle ij\rangle}[b_i^\dagger b_j + b_i b_j^\dagger] + V\sum_{\hexagon}(n_{\hexagon})^2$ (i and j are nearest-neighbor lattice sites; $b_i^\dagger$ and b_i are boson creation and annihilation operators,

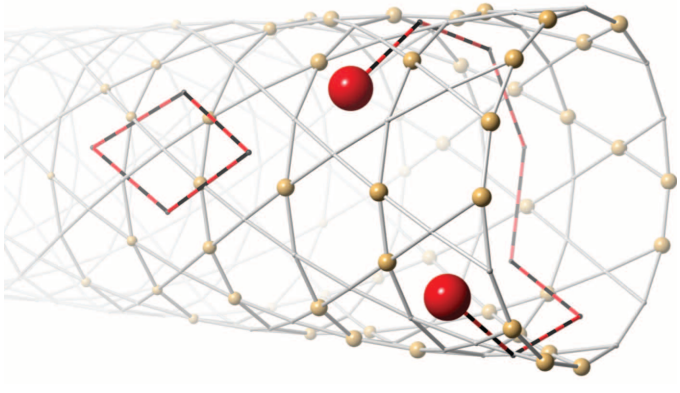

Fig. 1. A section of the toroidal kagome lattice simulation cell. Gold spheres label sites occupied by bosons in a representative configuration. Red spheres are fractional charges, marking "defect hexagons" (those that do not have three bosons per site). Defect hexagons are shown joined by an open string. We also show a representative closed string not associated with fractionalized particles.

[1]Theoretische Physik, ETH Zurich, 8093 Zurich, Switzerland. [2]Department of Physics and Astronomy, University of Waterloo, Waterloo, Ontario N2L 3G1, Canada. [3]Department of Physics, Duke University, Durham, NC 27708, USA. [4]Microsoft Research, Station Q, California NanoSystems Institute Building, University of California, Santa Barbara, CA 93106, USA.

*To whom correspondence should be addressed. E-mail: xhastings@gmail.com